NANO LETTERS

Letter

pubs.acs.org/NanoLett

Facet-Selective Epitaxy of Compound Semiconductors on Faceted Silicon Nanowires

Max N. Mankin,[†] Robert W. Day,[†] Ruixuan Gao,[†] You-Shin No,[†,∥] Sun-Kyung Kim,[†,⊥] Arthur A. McClelland,[§] David C. Bell,[§,‡] Hong-Gyu Park,[∥] and Charles M. Lieber*[,†,‡]

[†]Department of Chemistry and Chemical Biology, [‡]Harvard John A. Paulson School of Engineering and Applied Sciences, and [§]Center for Nanoscale Systems, Harvard University, Cambridge, Massachusetts 02138, United States

[∥]Department of Physics, Korea University, Seoul 136-701, Republic of Korea

Supporting Information

ABSTRACT: Integration of compound semiconductors with silicon (Si) has been a long-standing goal for the semiconductor industry, as direct band gap compound semiconductors offer, for example, attractive photonic properties not possible with Si devices. However, mismatches in lattice constant, thermal expansion coefficient, and polarity between Si and compound semiconductors render growth of epitaxial heterostructures challenging. Nanowires (NWs) are a promising platform for the integration of Si and compound semiconductors since their limited surface area can alleviate such material mismatch issues. Here, we demonstrate facet-selective growth of cadmium sulfide (CdS) on Si NWs. Aberration-corrected transmission electron microscopy analysis shows that crystalline CdS is grown epitaxially on the {111} and {110} surface facets of the Si NWs but that the Si{113} facets remain bare. Further analysis of CdS on Si NWs grown at higher deposition rates to yield a conformal shell reveals a thin oxide layer on the Si{113} facet. This observation and control experiments suggest that facet-selective growth is enabled by the formation of an oxide, which prevents subsequent shell growth on the Si{113} NW facets. Further studies of facet-selective epitaxial growth of CdS shells on micro-to-mesoscale wires, which allows tuning of the lateral width of the compound semiconductor layer without lithographic patterning, and InP shell growth on Si NWs demonstrate the generality of our growth technique. In addition, photoluminescence imaging and spectroscopy show that the epitaxial shells display strong and clean band edge emission, confirming their high photonic quality, and thus suggesting that facet-selective epitaxy on NW substrates represents a promising route to integration of compound semiconductors on Si.

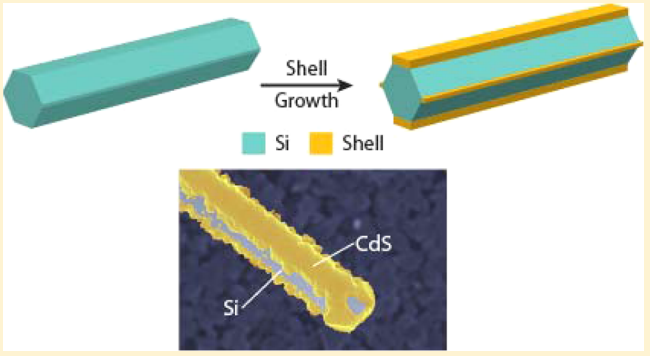

KEYWORDS: *Si/CdS, Si/InP, heterostructure nanowire, core/shell nanowire, facet-selective growth, epitaxial growth, selective area epitaxy, selective area growth, aspect ratio trapping*

Integration of Si and compound III−V or II−VI semiconductors is an attractive goal since such heterostructures could marry the attractive photonic properties of direct band gap compound semiconductors with Si devices.[1] However, mismatches in lattice constant, thermal expansion coefficient, and polarity between Si and compound semiconductors render growth of epitaxial heterostructures challenging.[2,3] Nanowires (NWs) represent a promising platform for the integration of Si and compound semiconductors since their small cross-sectional footprint and surface area can alleviate issues created by lattice, thermal, and polarity mismatches.[4,5] Thus far, several general strategies have been explored for compound semiconductor integration with Si in NWs. First, nanoparticle-catalyzed growth has yielded a variety of axially modulated group IV/III−V and II−VI NW heterostructures.[6−10] Second, III−V and II−VI NWs have been grown vertically on Si and germanium substrates[11−27] and on Si NWs, forming branched heterostructure NWs.[28] Lastly, there has been recent interest in core/shell heterostructure NWs, though the Si/III−V or II−VI core/shell interfaces are often difficult to control[29] or have not been characterized[30] and shells of high crystal quality with thicknesses beyond several nanometers have not been explored.[6,31,32]

Conceptually, facet-selective growth provides a means by which to reduce the interfacial area of mismatched materials since the growing layer is confined to the width of the facet on which it is deposited. We previously reported the synthesis of crystalline core/shell Si NWs, which grow in the ⟨211⟩ direction and whose surfaces are terminated by well-defined Si{111}, {113}, and {110} facets.[33] Studies have shown differences in growth rates of Si and Ge on the distinct Si

Received: May 1, 2015
Revised: May 27, 2015
Published: June 9, 2015

DOI: 10.1021/acs.nanolett.5b01721
Nano Lett. 2015, 15, 4776−4782

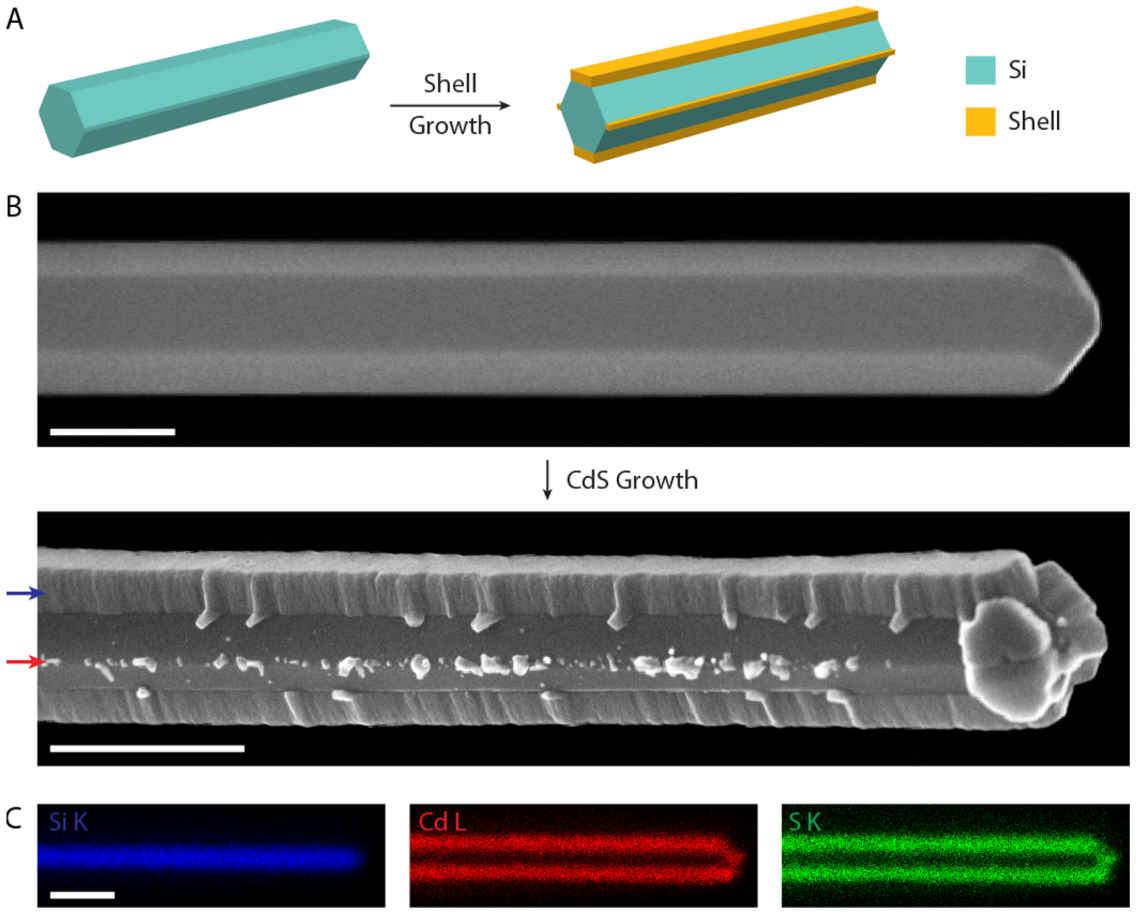

Figure 1. Facet-selective epitaxy on Si NWs. (A) Schematic depicting facet-selective growth of a shell material (orange) on faceted Si NWs (cyan). (B) Top, SEM image of a faceted Si NW before CdS growth. Bottom, SEM image of a Si/CdS heterostructure NW following CdS deposition. The blue and red arrows indicate CdS on Si{111} and {110} facets,[33] respectively. Scale bars, 500 nm. (C) STEM EDS elemental mapping of Si (blue), Cd (red), and S (green) of a NW oriented in the Si ⟨110⟩ zone axis. Scale bar, 500 nm.

surface facets, including (a) preferential Si growth on {113} facets in the presence of PH_3[34] and (b) controlled growth of Ge on Si{111} and {110} surfaces.[35] Here, we investigate the growth of CdS and InP shells, which are prototypical II−VI and III−V compounds, on Si NWs with well-defined facets, as shown schematically in Figure 1A.

Si NWs with well-developed facets and diameters from 200 to 400 nm (Figure 1B, top) were grown according to a previously described[33] procedure (Supporting Information). The growth substrate with the faceted Si NWs was dipped in aqueous buffered hydrofluoric acid (BHF) for 20 s to remove surface oxide, rinsed for 5 s in deionized water, and then submerged in liquid nitrogen to prevent collapse of the NWs via capillary forces during liquid water evaporation.[33] The frozen growth substrate was quickly transferred to the second zone of a 3-zone furnace, and the tube was evacuated to a base pressure of 50 mTorr; during this process, the ice sublimed. Once at base pressure, the furnace was purged three times each with Ar and H_2, and the pressure was set at ∼2.8 Torr with a flow rate of 20 sccm H_2. CdS was evaporated at 670−710 °C from zone 1 and deposited on the substrate in zone 2 at 450−550 °C for 5−40 min.

Scanning electron microscope (SEM) images of the Si NWs before and following CdS growth reveal several key features (Figure 1B). First, before growth, the Si NWs exhibit well-faceted structures similar to our previous report.[33] Second, following CdS growth, the SEM image shows CdS on distinct facets of the Si NWs. Specifically, the image shows that (i) the CdS forms a continuous stripe along the upper/lower facets and islands along the much narrower middle facet and that (ii) the intervening facets are free of deposited CdS. Comparison of the Si NW image to previous work[33] suggests that the continuous CdS growth occurs on Si NW {111} facets, while the islands form on {110} facets. Indeed, elemental mapping via energy-dispersive X-ray spectroscopy (EDS) in a scanning transmission electron microscope (STEM; Figure 1C) shows the spatial distributions of Si (blue), Cd (red), and S (green) from a Si NW oriented in the Si ⟨110⟩ zone axis. The elemental distribution matches the geometry shown in the schematic and the SEM images of Figure 1A,B, and moreover confirms that the CdS shells are primarily localized on the Si{111} facets.

To further characterize the facet-selective Si/CdS NW structure, we used plan-view aberration-corrected TEM (Figure 2). As depicted schematically in Figure 2A, plan-view TEM of facet-selective Si/CdS NWs oriented in the Si[111] zone axis allows for inspection of the Si-CdS{111} interface in plan-view and the Si-CdS{110} interface in cross-section. The TEM image of the Si-CdS{111} interface in plan-view (Figure 2B) shows a high contrast area on the left, due to CdS on the Si, while the lower contrast area on the right corresponds to exposed Si. The clear boundary between the Si and CdS in Figure 2B confirms that, in agreement with Figure 1, CdS

DOI: 10.1021/acs.nanolett.5b01721
Nano Lett. 2015, 15, 4776−4782

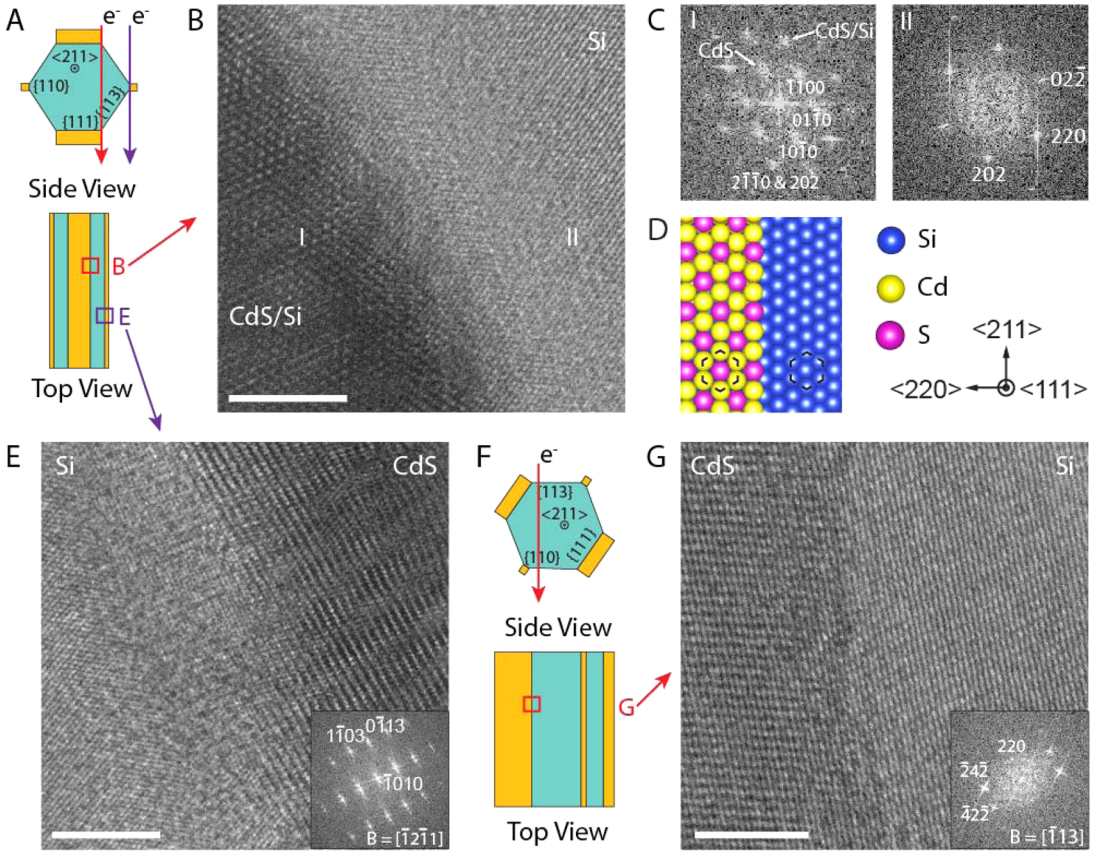

Figure 2. Plan-view TEM imaging of facet-selective Si/CdS heterostructure NWs. (A) Side- and top-view schematics of plan-view TEM imaging of facet-selective Si/CdS NWs oriented in the Si ⟨111⟩ zone axis. (B) Plan-view TEM image of the Si-CdS{111} interface showing the Si{113} facet (right) and CdS grown on the Si{111} facet (left). Scale bar, 4 nm. (C) FFTs from the CdS/Si and bare Si regions as depicted by (I) and (II) in (B), respectively. (D) Crystal structure model oriented in the Si ⟨111⟩ zone axis showing CdS epitaxially grown on a Si{111} facet next to a bare Si{113} facet. Crystal directions are indicated on the right. (E) Plan-view TEM image of the Si-CdS{110} interface showing the Si{113} facet (left) and CdS grown on the Si{110} facet (right). Scale bar, 4 nm. Inset, FFT from the CdS in the TEM image. (F) Side- and top-view schematics of plan-view TEM imaging of facet-selective Si/CdS NWs oriented in the Si ⟨113⟩ zone axis. (G) TEM image of a facet-selective Si/CdS NW in the Si ⟨113⟩ zone axis. Scale bar, 4 nm. Inset, FFT from the Si in the TEM image.

deposits selectively on the Si{111} surface facets of the Si NW and does not extend onto the Si{113} surface. In addition, a fast Fourier transform (FFT) of the exposed Si region (Figure 2C, II) yields a hexagonal pattern that can be indexed to Si ⟨111⟩ and is consistent with the imaging zone axis and facet orientation. The FFT of the CdS/Si region is a convolution of spots from two layers of CdS and the Si NW (Figure 2C, I), as expected from the imaging geometry. Importantly, it is possible to index the distinct CdS hexagonal spots to wurtzite CdS ⟨0001⟩ due to the presence of {1100} reflections in the FFT, which would not be present in a FFT of zinc-blende CdS. The orientations of Si and CdS spots with identical symmetries in the FFTs are equivalent, strongly suggesting that the orientation of the CdS is determined by epitaxy with the underlying Si{111} surface.

A crystal structure model based on the TEM image and FFT analyses of the Si ⟨111⟩/CdS ⟨0001⟩ zone axis (Figure 2D) depicts wurtzite phase CdS (left: sulfur, purple; Cd, yellow) growing epitaxially on a Si{111} surface adjacent to an exposed Si{113} facet (right, blue). As in their corresponding FFTs, both Si{111} and CdS{0001} have hexagonal symmetry, highlighted by the dashed hexagon in the model. Since the Si NW crystal structure is cubic whereas the CdS displays hexagonal (wurtzite) crystal symmetry, we note that, to our knowledge, this work presents the first report of clearly characterized heteroepitaxial polytypism, which is localized to specific facets of a NW.

Additional plan-view TEM imaging of the Si-CdS interface at the Si{110} facet (Figure 2E and schematic Figure 2A) shows that lattice fringes extend continuously from Si to the CdS, and moreover, there is no evidence for an interfacial layer. The FFT from this image (Figure 2E, inset) was indexed to CdS ⟨1211⟩, which indicates that the CdS ⟨1010⟩ and Si ⟨110⟩ directions are parallel. Moreover, CdS lattice fringes, with 0.37 nm spacing, are in agreement with CdS{1010} planes parallel to the Si{110} facet. Together, these observations confirm that CdS growth on the Si{110} facets was also epitaxial. We also tilted facet-selective Si/CdS NWs into the Si ⟨113⟩ zone axis (schematic, Figure 2F) to allow for plan-view imaging of the Si{113} facets. Figure 2G shows a TEM image of a Si{113} facet, where high contrast CdS grown on the adjacent Si{111} facet is observed on the left and the low contrast Si{113} facet is seen on the right. An FFT (Figure 2G, inset) from the Si region confirms the zone axis as Si ⟨113⟩. TEM imaging in the Si ⟨113⟩ zone axis does not yield any detectable CdS on the Si{113} facets.

We observe facet-selective CdS growth on Si NWs along the majority of the growth substrate. However, Si NWs closest to the upstream CdS source where the Cd/S reactant concentration is highest[36] (Figure 3A) show conformal CdS shells on the Si NW cores. To better probe the mechanism of facet-

DOI: 10.1021/acs.nanolett.5b01721
Nano Lett. 2015, 15, 4776−4782

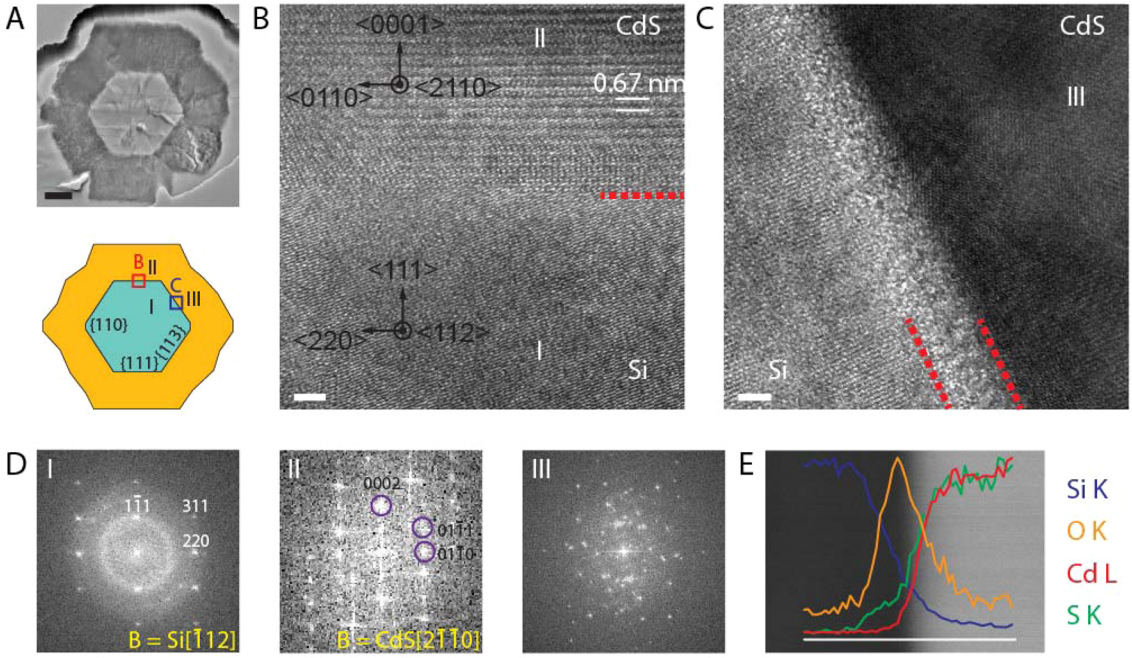

Figure 3. Cross-sectional TEM imaging of a conformal Si/CdS core/shell NW. (A) Top, TEM image of a cross-section from the conformal core/shell Si/CdS NW. Scale bar, 200 nm. Bottom, schematic depicting the geometry of the cross-section. B and C denote areas where the Si-CdS{111} and {113} interfaces are imaged at high magnification and presented in (B) and (C); I, II, and III refer to the FFT locations in (D). (B,C) Aberration-corrected TEM images of the Si-CdS (B) {111} and (C) {113} interfaces. Scale bars, 2 nm. Red dashed lines denote (B) the interface between Si and CdS and (C) an interfacial layer between the Si and CdS. (D) FFTs derived from ~35 × 35 nm^2 areas of (I) Si, (II) CdS grown on the Si{111} facet, and (III) CdS grown on the Si{113} facet. (E) STEM EDS line scan profile of Si (blue), O (orange), Cd (red), and S (green) through the Si-CdS{113} interface. The elemental intensity profiles are overlaid on a STEM image of the interface. The white line is ~17 nm long.

selective growth, we characterized the conformal core/shell Si/CdS NWs with cross-sectional TEM imaging (Supporting Information). A low magnification TEM view and schematic of the cross-section (Figure 3A, top and bottom) show the low contrast Si NW core with smooth surface facets, the concentric high contrast CdS shell, and an amorphous sacrificial carbon layer, which was deposited for sample preparation. The notch in the bottom right of the cross-section was caused by Ga FIB damage during cross-section thinning. The conformal Si/CdS NW displays smooth CdS surfaces parallel to the Si{111} facets but rough CdS surfaces parallel to the Si{113} facets, as shown schematically in the bottom of Figure 3A.

In addition, higher resolution TEM images of the Si-CdS{111} interface (Figure 3B) show continuous lattice fringes from the Si to the CdS and no interfacial layer between the Si NW and CdS. We index FFTs of the Si (Figure 3D, I) and CdS (Figure 3D, II) to Si ⟨211⟩ and CdS ⟨2110⟩, respectively. Both FFTs and their respective crystal directions have identical symmetry. The Si[211] crystal direction matches the previously reported growth direction of our Si NWs.[33] Moreover, the periodically spaced 0.67 nm CdS lattice fringes parallel to the Si-CdS{111} interface show that the CdS growth direction normal to the Si{111} facet is ⟨0001⟩. Fourier-filtered TEM images of the Si-CdS{111} interface (Figure S1) show misfit dislocations ~4 nm from the interface. Additionally, TEM images of the CdS recorded greater than ~30 nm from the Si-CdS {111} interface (Figure S1) reveal that the CdS is practically free of defects. We note that no evidence for antiphase boundaries in the CdS layer[37] were observed in our TEM imaging studies; however, we acknowledge that this does not eliminate the possibility of such defects, particularly along a given CdS on Si{111} facet. Taken together, this evidence confirms the epitaxial relationship between the Si and CdS on the Si{111} interface, consistent with the plan-view TEM analysis of the facet-selective Si/CdS NWs in Figure 2.

Interestingly, TEM images of the Si-CdS{113} interface (Figure 3C) reveal a ~3 nm layer, which interrupts the Si (left) and CdS (right) lattice fringes and which is devoid of structural features and fringes. An FFT recorded from the CdS (Figure 3D, III) reveals randomly angled spot patterns, indicating that the CdS in this region is polycrystalline, in agreement with the rough CdS shell surface observed parallel to the Si{113} surfaces.[36] Together, this evidence indicates that the interfacial layer is amorphous. An aberration-corrected STEM EDS line scan (Figure 3E) reveals the presence of oxygen, consistent with amorphous silicon oxide in the interfacial layer separating Si and CdS.

Based on the above data, we propose that facet-selective growth of CdS on the Si{111} and {110} facets can be attributed at least in part to a passivating amorphous silicon oxide layer on the Si{113} facets. Although oxide is removed from the Si NWs immediately prior to placement in the CdS growth reactor, previous literature has reported that the sticking coefficient of water is 2 orders of magnitude higher for Si{113} than for Si{111}[38,39] and that adsorbed water decomposes to form silicon surface oxide at temperatures comparable to our CdS growth.[40,41] The continuous lattice fringes observed at the {111} interface (Figure 3B) suggest that oxygen-containing impurities are not significantly incorporated into this interface. However, given the base pressure of our growth apparatus, it is possible that residual water/oxygen can lead to oxide formation on Si{113} prior to deposition of CdS. Since there is no chemical difference between the Si NWs upstream and downstream (relative to the CdS reactant source), the

DOI: 10.1021/acs.nanolett.5b01721
Nano Lett. 2015, 15, 4776−4782

Si{113} oxide forms on NWs in both positions. However, the difference in CdS flux between upstream and downstream locations results in facet-selectivity. Upstream, CdS shells grow conformally because the higher reactant flux precludes sufficient time for diffusion and/or desorption. This suggestion is consistent with the ~1−2 μm CdS shells on upstream Si NWs (Figure 3A). In contrast, the lower CdS flux at the downstream position[36] allows for diffusion and/or desorption from the {113} oxide before incorporation into the shell, thereby yielding facet-selective CdS growth.

To better understand the role of oxide in the growth of CdS on Si NWs, we grew CdS on faceted Si NWs without removal of the Si NW native surface oxide prior to CdS deposition (Figure S2). In the upstream position, SEM images show conformal CdS shells with rough surfaces that are consistent with deposition of a fully polycrystalline shell. This contrasts with the well-developed {0001} facets observed when the native surface oxide was removed immediately prior to growth (Figure 3A). In the downstream position, SEM images show that no continuous CdS shell forms on any facets of the Si NWs with native oxide, in contrast to the facet-selective growth under the same conditions when the oxide was removed prior to growth (Figure 1B).

We note an analogy between our proposed mechanism and selective area epitaxy/growth (SAE/SAG), which have been implemented to epitaxially grow group IV, II−VI, or III−V films[42−47] and NWs[23−27] on lattice-mismatched substrates. In SAE, an amorphous oxide or nitride mask layer is deposited on a substrate and holes or trenches are patterned in the mask layer. Precursor flux is controlled such that long adatom diffusion lengths result in selective film growth on the exposed substrate rather than on the mask. However, we note that the novelty of facet-selective epitaxy on NW substrates stems from (1) intrinsic "patterning" of the substrate with faceted NW structures and (2) the natural formation of an oxide due to the difference in facet reactivity without the need for any lithographic patterning.

Therefore, our facet-selective epitaxy approach should be general for 1D Si structures and likely other NWs as well. To first evaluate this generality we deposited CdS on micrometer diameter Si wires (Figure 4A,B). SEM images of the resultant heterostructures reveal facet-selective growth of CdS on the Si{111} facets. Second, we demonstrate the generality toward other shell materials by growing indium phosphide (InP) on faceted Si NWs. SEM imaging of InP growth carried out in a manner similar to the deposition of CdS (Supporting Information) on Si NWs (Figure 4C) confirms that InP islands grow selectively on the Si{111} facets and that the Si{113} facets remain free of InP.

Finally, we characterized the optical properties of the facet-selective Si/CdS heterostructure NWs. A scanning confocal photoluminescence image of facet-selective Si/CdS heterostructure NWs randomly dispersed on a quartz substrate (Figure 5A) reveals strong green emission. Comparison of NW positions determined by bright-field and photoluminescence images demonstrates that every NW in the field of view exhibits strong luminescence. Moreover, a representative room temperature photoluminescence spectrum from a single Si/CdS NW (Figure 5B) shows a symmetric emission profile, featuring strong band-edge emission at ~514 nm (2.4 eV), which is consistent with high quality crystalline bulk CdS. We do not observe any strong emission except for the band-edge peak, indicating that the CdS on the faceted Si NWs has a relatively

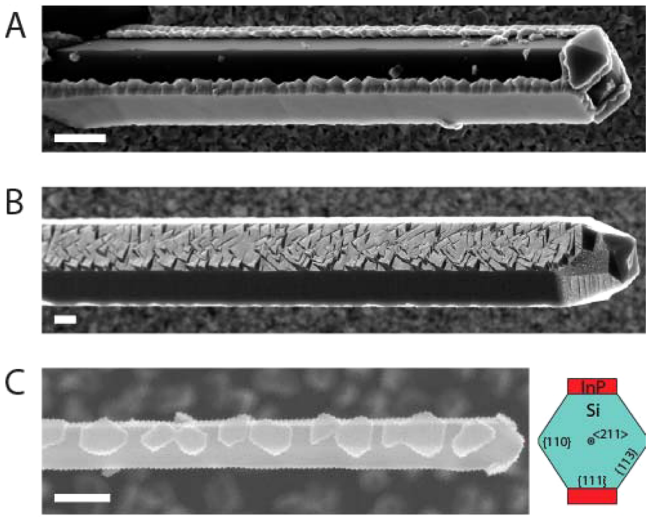

Figure 4. Generality of facet-selective epitaxy. (A,B) Facet-selective CdS growth on Si wires of various sizes. SEM image of Si/CdS heterostructure wires with diameters of ca. (A) 3 and (B) 10 μm. Scale bars, 2 μm. (C) Left, SEM image of a Si/InP heterostructure NW. Scale bar, 400 nm. Right, schematic depicting the crystallography of the facet-selective Si/InP structure.

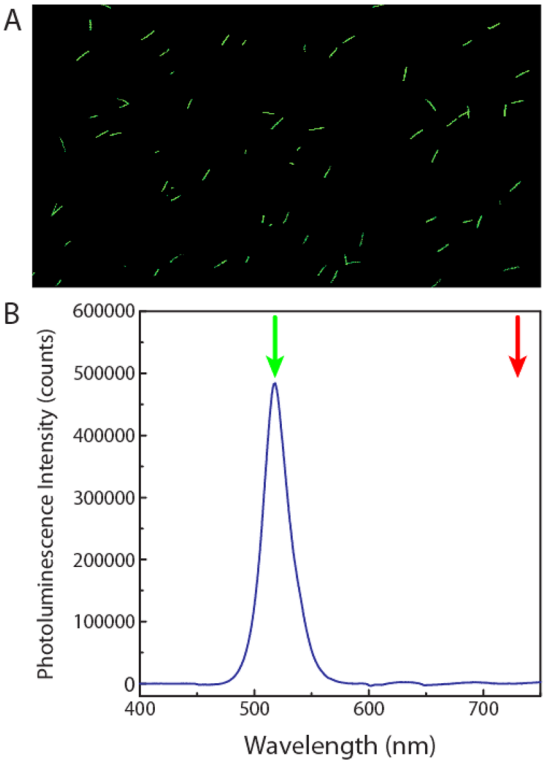

Figure 5. Optical characterization of the facet-selective Si/CdS heterostructure NWs. (A) Scanning confocal photoluminescence image of facet-selective Si/CdS heterostructure NWs randomly dispersed on a quartz substrate. (B) Room temperature photoluminescence spectrum from a single Si/CdS NW. The green arrow indicates the wavelength of band-edge (514 nm; 2.4 eV) emission from high quality crystalline bulk CdS; the red arrow indicates the previously reported wavelength of emission due to S-vacancy defects (~730 nm; 1.7 eV).[48]

low concentration of S-vacancy defects,[48] does not display optical characteristics indicative of quantum confinement,[49] and

DOI: 10.1021/acs.nanolett.5b01721
Nano Lett. 2015, 15, 4776−4782

is of high optical quality. Therefore, facet-selective Si/CdS NWs show potential for integration of compound semiconductors with Si for (opto)electronics.

In summary, we have demonstrated facet-selective growth of CdS on Si NWs. Aberration-corrected transmission electron microscopy analyses have shown that the crystalline CdS is grown epitaxially on the {111} and {110} surface facets of the Si NWs and that the Si{113} facets remain bare. Further analysis of conformal CdS shells on Si NWs grown at higher deposition rates revealed a thin oxide layer on the Si{113} facet, suggesting that the facet-selective growth is enabled by the formation of an oxide, which prevents subsequent shell growth on the Si{113} NW facets. Further studies of the generality of facet-selective epitaxial growth demonstrated the potential of the technique on micro-to-mesoscale wires, which allows tuning of the lateral width of the compound semiconductor layer without lithographic patterning and InP shell growth on Si NWs. In addition, photoluminescence imaging and spectroscopy show that the epitaxial shells display strong and clean band edge emission, thus confirming their high photonic quality, suggesting that facet selective epitaxy on 1D Si structures could serve as a unique platform for integrating compound semiconductors with group IV materials in (opto)electronics.

■ ASSOCIATED CONTENT

Supporting Information

Detailed description of experimental methods and additional figures. The Supporting Information is available free of charge on the ACS Publications website at DOI: 10.1021/acs.nanolett.5b01721.

■ AUTHOR INFORMATION

Corresponding Author

*E-mail: cml@cmliris.harvard.edu.

Present Address

[⊥]Department of Applied Physics, Kyung Hee University, Gyeonggi-do 446-701, Republic of Korea.

Notes

The authors declare no competing financial interest.

■ ACKNOWLEDGMENTS

The authors gratefully acknowledge C. Aspetti, R. Agarwal, J. Liu, and D. Fu for guidance with optical measurements; N. Antoniou, A. Magyar, and A. Graham for assistance with electron microscopy; Hitachi for STEM use; and T.-M. Fu, T. Kempa, and X. Jiang for fruitful discussions. M.N.M. acknowledges a Fannie and John Hertz Foundation Graduate Fellowship and a NSF Graduate Research Fellowship. R.W.D acknowledges a NSF Graduate Research Fellowship. R.G. acknowledges the support of a Japan Student Services Organization Graduate Research Fellowship. D.C.B. acknowledges NSF awards NSF DMR-1040243 and NSF DMR-1108382. H.-G.P. acknowledges support from the National Research Foundation of Korea (NRF) grant funded by the Korea government (MSIP) (No. 2009-0081565). This work was performed in part at the Center for Nanoscale Systems (CNS), a member of the National Nanotechnology Infrastructure Network (NNIN), which is supported by the National Science Foundation under NSF award no. ECS-0335765. CNS is part of Harvard University.

■ REFERENCES

(1) Li, T.; Mastro, M.; Dadger, A. *III−V Compound Semiconductors: Integration with Silicon-Based Microelectronics*; CRC Press: Boca Raton, FL, 2011.
(2) del Alamo, J. A. *Nature* **2011**, *479*, 317−323.
(3) Liu, C. W.; Östling, M.; Hannon, J. B. *MRS Bull.* **2014**, *39*, 658−662.
(4) Hyun, J. K.; Zhang, S.; Lauhon, L. J. *Annu. Rev. Mater. Res.* **2013**, *43*, 451−479.
(5) Tsivion, D.; Joselevich, E. *Nano Lett.* **2013**, *13*, 5491−5496.
(6) Conesa-Boj, S.; Dunand, S.; Russo-Averchi, E.; Heissa, M.; Ruffer, D.; Wyrschb, N.; Ballif, C.; Fontcuberta i Morral, A. *Nanoscale* **2013**, *5*, 9633−9639.
(7) Gamalski, A. D.; Perea, D. E.; Yoo, J.; Li, N.; Olszta, M. J.; Colby, R.; Schreiber, D. K.; Ducati, C.; Picraux, S. T.; Hofmann, S. *ACS Nano* **2013**, *7*, 7689−7697.
(8) Hillerich, K.; Dick, K. A.; Wen, C.-Y.; Reuter, M. C.; Kodambaka, S.; Ross, F. M. *Nano Lett.* **2013**, *13*, 903−908.
(9) Dick, K. A.; Kodambaka, S.; Reuter, M. C.; Deppert, K.; Samuelson, L.; Seifert, W.; Wallenberg, L. R.; Ross, F. M. *Nano Lett.* **2007**, *7*, 1817−1822.
(10) Hocevar, M.; Immink, G.; Verheijen, M.; Akopian, N.; Zwiller, V.; Kouwenhoven, L.; Bakkers, E. *Nat. Commun.* **2012**, *3*, 1266−1−6.
(11) Tomioka, K.; Motohisa, J.; Hara, S.; Fukui, T. *Nano Lett.* **2008**, *8*, 3475−3480.
(12) Plissard, S.; Dick, K. A.; Larrieu, G.; Godey, S.; Addad, A.; Wallart, X.; Caroff, P. *Nanotechnology* **2010**, *21*, 385602.
(13) Plissard, S.; Dick, K. A.; Wallart, X.; Caroff, P. *Appl. Phys. Lett.* **2010**, *96*, 121901.
(14) Ng, K. W.; Ko, W. S.; Tran, T.-T. D.; Chen, R.; Nazarenko, M. V.; Lu, F.; Dubrovskii, V. G.; Kamp, M.; Forchel, A.; Chang-Hasnain, C. J. *ACS Nano* **2013**, *7*, 100−107.
(15) Ng, K. W.; Tran, T.-T. D.; Ko, W. S.; Chen, R.; Lu, F.; Chang-Hasnain, C. J. *Nano Lett.* **2013**, *13*, 5931−5937.
(16) Chen, R.; Tran, T.-T. D.; Ng, K. W.; Ko, W. S.; Chuang, L. C.; Sedgwick, F. G.; Chang-Hasnain, C. J. *Nat. Photonics* **2011**, *5*, 170−175.
(17) Li, K.; Sun, H.; Ren, F.; Ng, K. W.; Tran, T.-T. D.; Chen, R.; Chang-Hasnain, C. J. *Nano Lett.* **2014**, *14*, 183−190.
(18) Martensson, T.; Svensson, C. P. T.; Wacaser, B. A.; Larsson, M. W.; Seifert, W.; Deppert, K.; Gustafsson, A.; Wallenberg, L. R.; Samuelson, L. *Nano Lett.* **2004**, *4*, 1987−1990.
(19) Uccelli, E.; Arbiol, J.; Magen, C.; Krogstrup, P.; Russo-Averchi, E.; Heiss, M.; Mugny, G.; Morier-Genoud, F.; Nygård, J.; Morante, J. R.; Fontcuberta i Morral, A. *Nano Lett.* **2011**, *11*, 3827−3832.
(20) We, W.; Bao, X.-Y.; Soci, C.; Ding, Y.; Wang, Z.-L.; Wang, D. *Nano Lett.* **2009**, *9*, 2926−2934.
(21) Shin, J. C.; Lee, A.; Mohseni, P. K.; Kim, D. Y.; Yu, L.; Kim, J. H.; Kim, H. J.; Choi, W. J.; Wasserman, D.; Choi, K. J.; Li, X. *ACS Nano* **2013**, *7*, 5463−5471.
(22) Heiss, M.; Russo-Averchi, E.; Dalmau-Mallorquí, A.; G Tütüncüoğlu, G.; Matteini, F.; Rüffer, D.; Conesa-Boj, S.; Demichel, O.; Alarcon-Lladó, E.; Fontcuberta i Morral, A. *Nanotechnology* **2014**, *25*, 014015.
(23) Tomioka, K.; Ikejiri, K.; Tanaka, T.; Motohisa, J.; Hara, S.; Hiruma, K.; Fukui, T. *J. Mater. Res.* **2011**, *26*, 2127−2141.
(24) Tomioka, K.; Yoshimura, M.; Fukui, T. *Nature* **2012**, *488*, 189−192.
(25) Tomioka, K.; Tanaka, T.; Hara, S.; Hiruma, K.; Fukui, T. *IEEE J. Sel. Top. Quant. Electron.* **2011**, *17*, 1112−1129.
(26) Tomioka, K.; Motohisa, J.; Hara, S.; Hiruma, K.; Fukui, T. *Nano Lett.* **2010**, *10*, 1639−1644.
(27) Kawaguchi, K.; Sudo, H.; Matsuda, M.; Takemoto, K.; Yamamoto, T.; Arakawa, Y. *Appl. Phys. Lett.* **2015**, *106*, 012107.
(28) Jiang, X.; Tian, B.; Xiang, J.; Qian, F.; Zheng, G.; Wang, H.; Mai, L.; Lieber, C. M. *Proc. Natl. Acad. Sci. U.S.A.* **2011**, *108*, 12212−12216.
(29) Hayden, O.; Greytak, A. B.; Bell, D. C. *Adv. Mater.* **2005**, *17*, 701−704.

DOI: 10.1021/acs.nanolett.5b01721
Nano Lett. 2015, 15, 4776−4782

(30) Manna, S.; Das, S.; Mondal, S. P.; Singha, R.; Ray, S. K. *J. Phys. Chem. C* **2012**, *116*, 7126−7133.
(31) Conesa-Boj, S.; Boioli, F.; Russo-Averchi, E.; Dunand, S.; Heiss, M.; Rüffer, D.; Wyrsch, N.; Ballif, C.; Leo Miglio, L.; Fontcuberta i Morral, A. *Nano Lett.* **2014**, *14*, 1859−1864.
(32) Algra, R. E.; Hocevar, M.; Verheijen, M. A.; Zardo, I.; Immink, G. G. W.; van Enckevort, W. J. P.; Abstreiter, G.; Kouwenhoven, L. P.; Vlieg, E.; Bakkers, E. P. A. M. *Nano Lett.* **2011**, *11*, 1690−1694.
(33) Kempa, T. J.; Cahoon, J. F.; Kim, S.-K.; Day, R. W.; Bell, D. C.; Park, H.-G.; Lieber, C. M. *Proc. Natl. Acad. Sci. U.S.A.* **2012**, *109*, 1407−1412.
(34) Kim, S.-K.; Day, R. W.; Cahoon, J. F.; Kempa, T. J.; Song, K.-D.; Park, H.-G.; Lieber, C. M. *Nano Lett.* **2012**, *12*, 4971−4976.
(35) Kempa, T. J.; Kim, S.-K.; Day, R. W.; Park, H.-G.; Nocera, D. G.; Lieber, C. M. *J. Am. Chem. Soc.* **2013**, *135*, 18354−18357.
(36) Smith, D. L. *Thin-Film Deposition: Principles and Practice*; McGraw Hill: New York, 1995.
(37) Fang, S. F.; Adomi, K.; Iyer, S.; Morkoc, H.; Zabel, H.; Choi, C.; Otsuka, N. *Appl. Phys. Lett.* **1990**, *68*, R31−R58.
(38) Jacobi, K.; Myler, U. *Surf. Sci.* **1993**, *284*, 223−235.
(39) Mussig, H.-J.; Dabrowski, J.; Ehwald, K.-E.; Gaworzewski, P.; Huber, A.; Lambert, U. *Microelectron. Eng.* **2001**, *56*, 195−203.
(40) Scholz, S. M.; Jacobi, K. *Surf. Sci.* **1996**, *369*, 117−125.
(41) Ranke, W.; Xing, Y. R. *Surf. Sci.* **1997**, *381*, 1−11.
(42) Lourdudoss, S. *Curr. Opin. Solid State Mater. Sci.* **2012**, *16*, 91−99.
(43) Scholz, F. *Semicond. Sci. Technol.* **2012**, *27*, 024002.
(44) Fiorenza, J. G.; Park, J.-S.; Hydrick, J.; Li, J.; Curtin, M.; Carroll, M.; Lochtefeld, A. *ECS Trans.* **2010**, *33*, 963−976.
(45) Wu, Y. Q.; Xu, M.; Ye, P. D.; Cheng, Z.; Li, J.; Park, J.-S.; Hydrick, J.; Bai, J.; Carroll, M.; Fiorenza, J. G.; Lochtefeld, A. *Appl. Phys. Lett.* **2008**, *93*, 242106.
(46) Langdo, T. A.; Leitz, C. W.; Currie, M. T.; Fitzgerald, E. A.; Lochtefeld, A.; Antoniadis, D. A. *Appl. Phys. Lett.* **2000**, *76*, 3700−3702.
(47) Michel, J.; Liu, J.; Kimerling, L. C. *Nat. Photonics* **2010**, *4*, 527−534.
(48) Aguilar-Hernandez, J.; Contreras-Puente, G.; Morales-Acevedo, A.; Vigil-Galan, O.; Cruz-Gandarilla, F.; Vidal-Larramendi, J.; Escamilla-Esquivel, A.; Hernandez-Contreras, H.; Hesiquio-Garduno, M.; Arias-Carbajal, A.; Chavarria-Castaneda, M.; Arriaga-Mejia, G. *Semicond. Sci. Technol.* **2003**, *18*, 111−114.
(49) Vossmeyer, T.; Katsikas, L.; Giersig, M.; Popovic, I. G.; Diesner, K.; Chemseddine, A.; Eychmuller, A.; Weller, H. *J. Phys. Chem.* **1994**, *98*, 7665−7673.

DOI: 10.1021/acs.nanolett.5b01721
Nano Lett. 2015, 15, 4776−4782